REPORT

UV Resonance Raman Spectroscopy

for Analytical, Physical, and Biophysical Chemistry

Part 2

Sanford A. Asher
Department of Chemistry
University of Pittsburgh
Pittsburgh, PA 15260

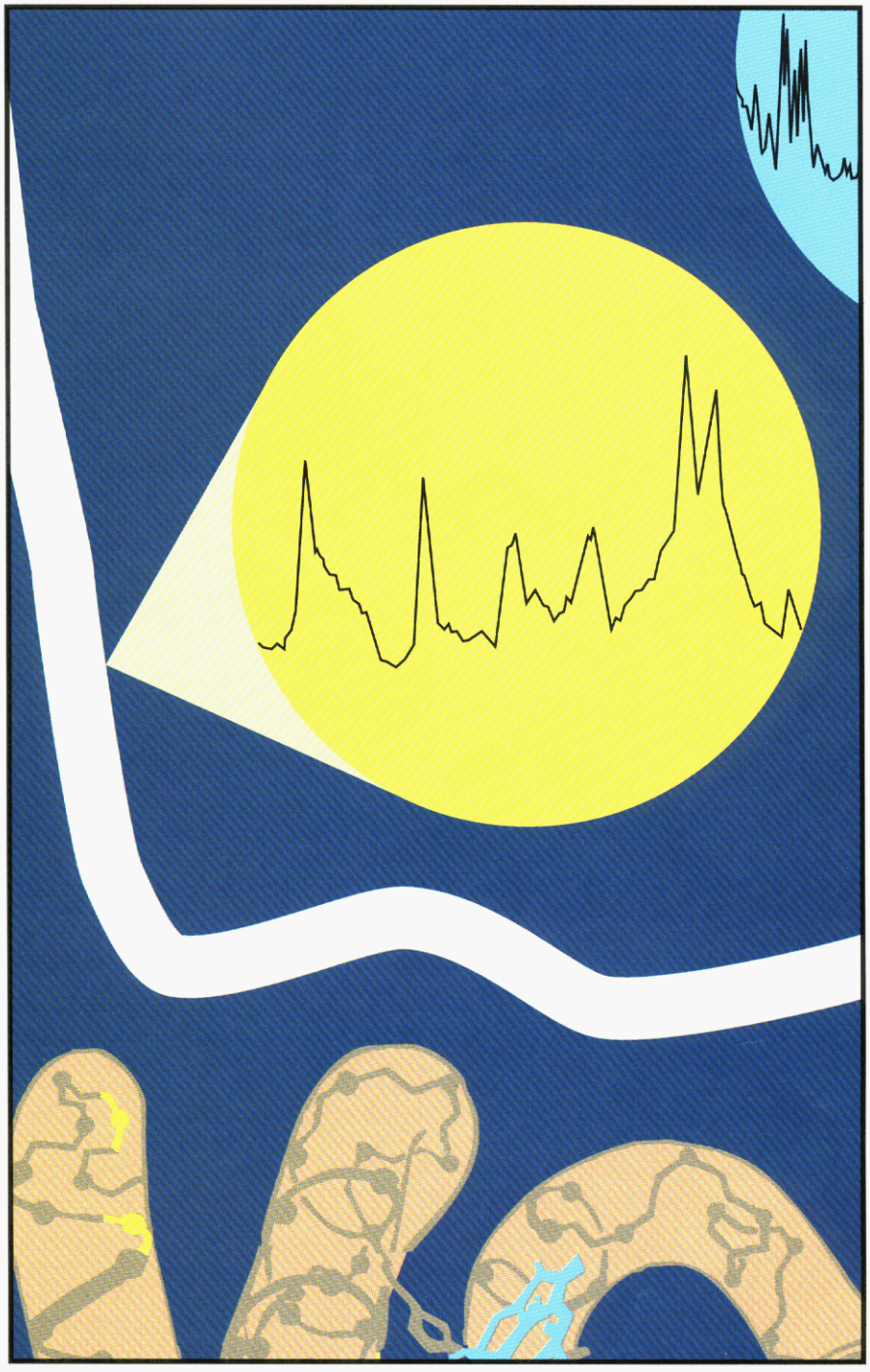

In Part 1 of this series (*1*), the history, phenomenology, instrumentation, and fundamental applications of UV resonance Raman spectroscopy were discussed. In Part 2, analytical applications, biological studies, new methods, and future developments complete the discussion.

Analytical applications

The ability of UV resonance Raman spectroscopy to selectively examine the vibrational behavior of particular species in complex mixtures makes the technique uniquely important for analytical applications. Selectivity is determined by the relative Raman cross sections of the analyte compared to other species present in the sample. Sensitivity depends on the relative intensities of the analyte Raman bands compared with overlapping, interfering Raman bands and emissions from the sample. Fluorescence interference does not normally occur in condensed phases with UV excitation below 260 nm; those species that have their lowest singlet state below 260 nm have vanishingly low fluorescence quantum yields because they are flexible and return to the ground state through nonradiative processes (*2*).

Polycyclic aromatic hydrocarbons (PAHs) are the most intense Raman scatterers (*3–6*). The UV-Raman spectra of a series of PAHs in Figure 1 show numerous bands that are indicative of fused-ring systems. The vibrations that are enhanced are mostly symmetric in-plane ring breathing vibrations. The spectra, though similar, differ enough to identify the ring system. Although aliphatic ring substituents perturb the spectra, the enhanced vibrations remain predominantly ring breath-

0003-2700/93/0365-201A/$04.00/0

ing modes; peripheral substituent vibrations are not generally observed unless they are conjugated into the aromatic π network (*3*). The major changes that occur upon ring substitution involve alterations in relative intensities and frequency shifts, which depend on the substitution pattern in the different compounds. The Raman cross sections are large enough that it is easy to study these analytes at ppm and ppb concentrations (*3, 6*).

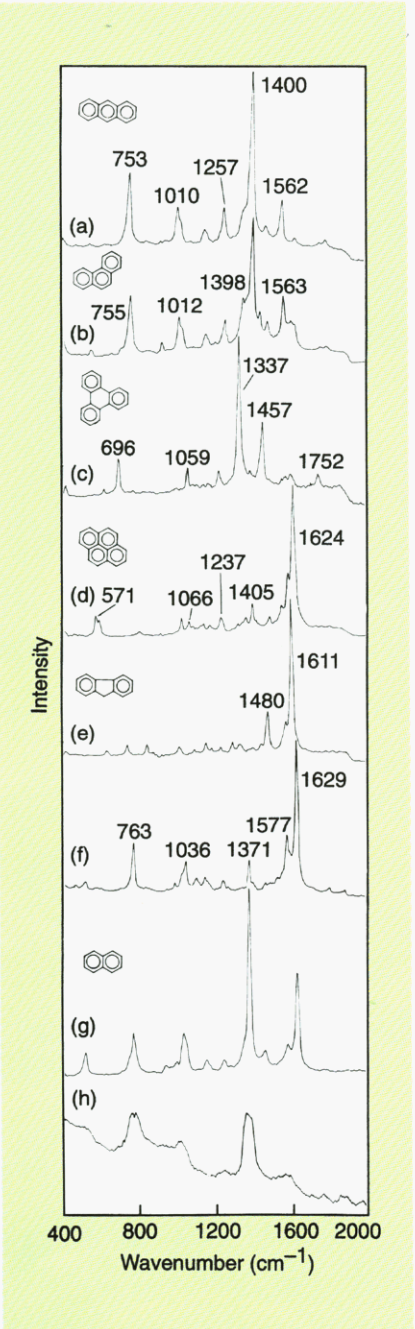

Figure 1. Resonance Raman spectra of 5-mM solutions of PAHs dissolved in acetonitrile and excited at 255 nm.

(a) Anthracene. (b) Phenanthrene. (c) Triphenylene. (d) Pyrene. (e) Fluorene. Napthalene excited at (f) 255 nm, (g) 235 nm, and (h) 220 nm. (Adapted with permission from Reference 7.)

Figure 2 shows the UV absorption spectra of a series of PAH ring systems. The absorption derives from in-plane $\pi \rightarrow \pi^*$ transitions of the ring systems. Most of the substructure observed for each band derives from vibronic Franck–Condon overlaps involving particular in-plane ring vibrations. These are the same vibrations that are most enhanced in the resonance Raman spectra.

The Raman intensities vary with excitation frequency and these excitation profiles often qualitatively follow the absorption spectra. For example, Figure 3 shows the resonance Raman spectra of pyrene excited at different wavelengths within its S_4 absorption band (*6*). The shaded bands, from acetonitrile, show little change in Raman cross section as the excitation wavelength is varied.

Figure 4 shows the absorption bandshape of the pyrene S_4 electronic transition and the Raman excitation profiles for some of the observed bands. The 592 and 1632 cm^{-1} bands show Raman cross sections > 50 Barns/molc sr at ~ 240 nm at the excitation profile maximum. Off the maximum, the cross sections decrease quickly. The excitation profile bandwidths and bandshapes differ between Raman bands; this dependence is related to the Franck–Condon activity of the vibration in the electronic transition and other subtle issues. These distinct excitation profiles lead to excitation frequency-dependent Raman spectra that differ in both absolute and relative intensities, as evident from the data in Figures 3 and 4.

We demonstrated that resonance Raman excitation of coal-derived liquid distillates (*2, 5, 7*) would selectively excite PAH species. For example, excitation at 244 nm selectively excites pyrene-type species, whereas excitation at shorter wavelengths selects for smaller aromatic ring systems. Recently we examined the residue, dissolved in tetrahydrofuran (THF), that remained after distillation of a coal-derived liquid. Using the new continuous-wave UV frequency doubled Ar^+ laser, we detected PAHs and unsaturation in THF solutions as well as in spinning dried films and pressed powders.

The Raman spectra showed peaks at ~ 1630 and 1400 cm^{-1}, regions expected for PAH in-plane ring vibrations. The coal residue samples differed in their origin or in their processing conditions. Although our results are still preliminary, we observed differences in the bandwidths, frequencies, and relative Raman intensities between samples. These differences provide sample composition information. This approach shows promise for studying PAHs in coal liquid and petroleum samples.

PAHs are of interest because of their ubiquity in the environment and because many of them are highly carcinogenic, making identification and quantitation in both environ-

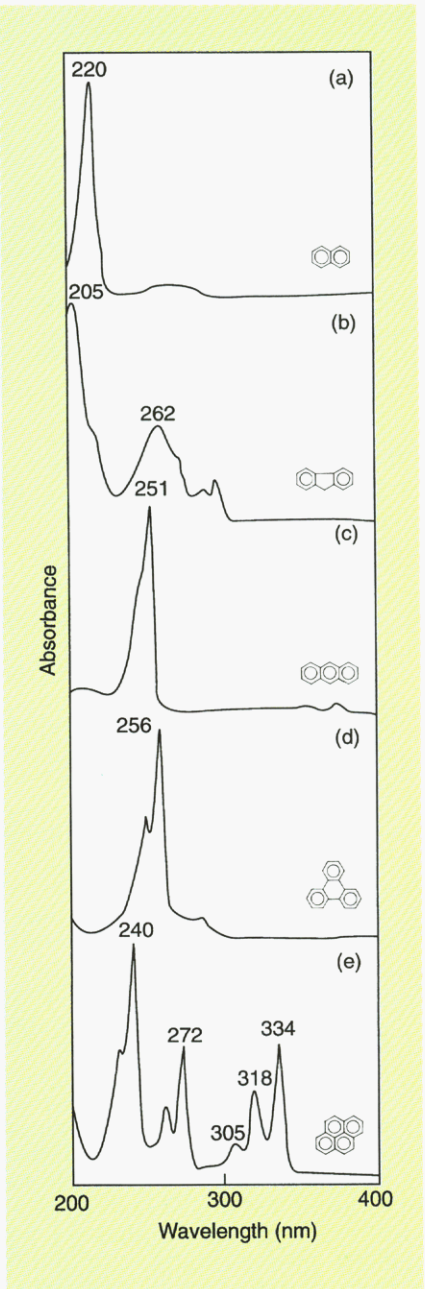

Figure 2. UV absorption spectra of PAHs dissolved in acetonitrile.

(a) Naphthalene. (b) Fluorene. (c) Anthracene. (d) Triphenylene. (e) Pyrene. (Adapted from Reference 4.)

mental and biological samples a high priority. Indeed, it would be especially useful to monitor PAHs during the events associated with chemical carcinogenesis.

Figure 5 shows the Raman spectra of a calf thymus DNA sample (*8*) to which pyrene was added until a concentration of ~ 1 molecule pyrene per 70 nucleic acid base pairs was reached. Excitation at 244 nm strongly enhances the nucleic acid base vibrations. The nucleic acid bands are evident as labeled peaks that derive from cytosine (C), guanine (G), or adenine (A).

The lower spectrum in Figure 5a shows pyrene peaks (e.g., 1632 cm^{-1}) comparable in intensity to the DNA bands. This occurs because, in this case, pyrene intercalates between DNA base pairs. Excitonic interactions between the pyrene and nucleic acids cause a large hypochromic absorption change that results in an even larger Raman hypochromism (the Raman cross sections scale as the square of the molar absorptivity).

On addition of sodium dodecyl sulfate (SDS), the pyrene partitions into the SDS micelles and the pyrene bands at 1632 and 592 cm^{-1} gain intensity, dominating the Raman spectra. The difference spectra in Figure 5b show that it is easy to monitor either the pyrene intercalated between the nucleic acid bases or the pyrene within SDS micelles.

The vibrational frequencies give information on interactions between the pyrene and the DNA, whereas the cross sections report on electronic interactions between the S_4 pyrene electronic transition and the nucleic acid base transitions. These interactions depend strongly on the binding geometry. Thus, UV-Raman spectroscopy appears to be useful for studying the binding of PAHs to DNA.

Our choice to begin PAH–DNA binding studies with pyrene was motivated by our extensive studies of

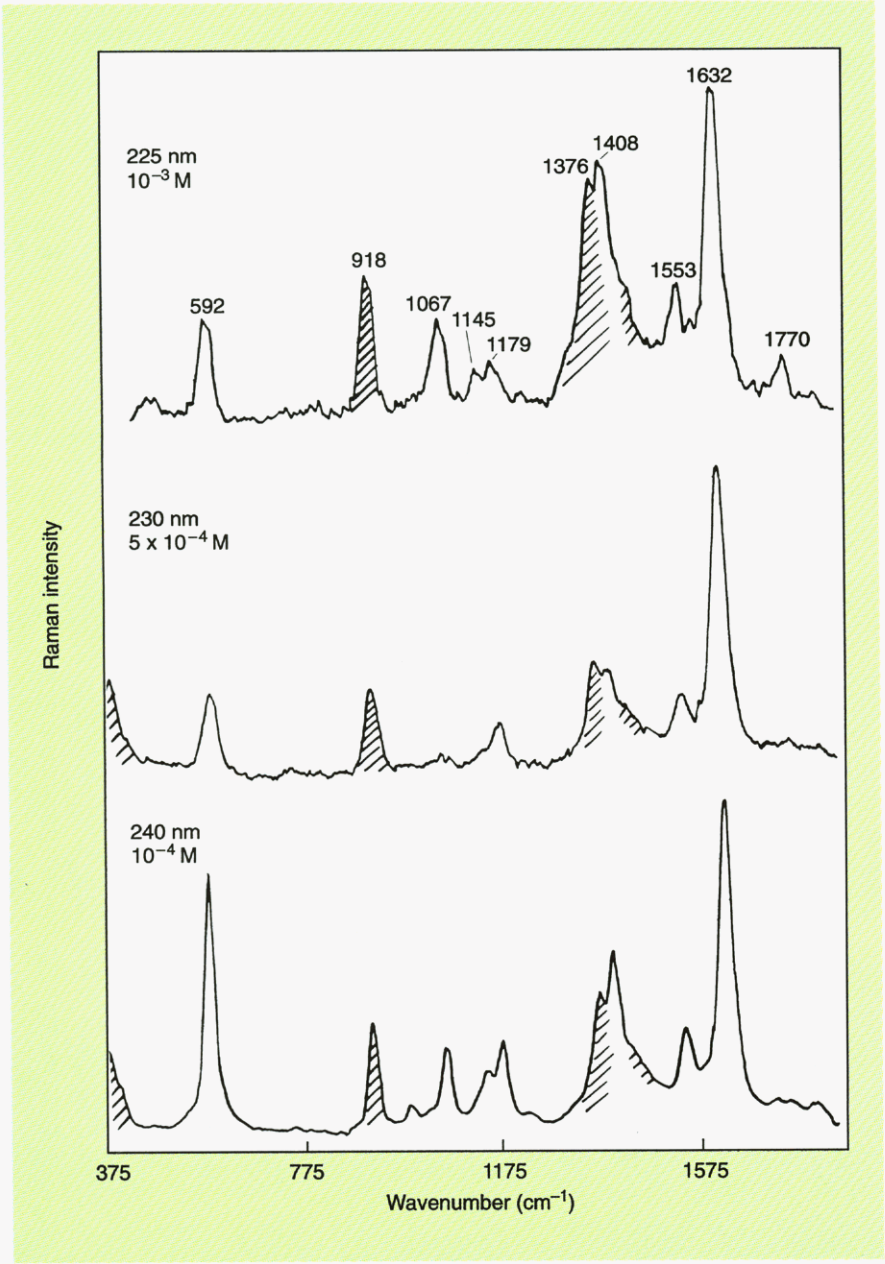

Figure 3. Resonance Raman spectra of pyrene excited in the S_4 electronic transition at different excitation wavelengths.

Acetonitrile solvent bands are shaded. The intensities of the pyrene bands relative to acetonitrile are affected by saturation.

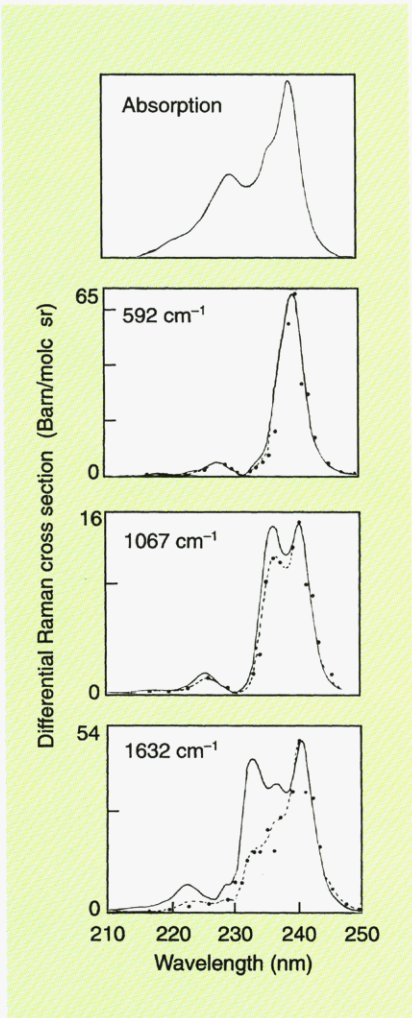

Figure 4. Pyrene S_4 absorption spectrum and Raman excitation profile of various bands.

The dots are the experimentally observed Raman cross sections; the solid and dashed lines are theoretically calculated excitation profiles from the absorption bandshape. (Adapted with permission from Reference 6.)

pyrene spectroscopy (*6*), the knowledge that pyrene itself is not carcinogenic, and the fact that the binding mode of pyrene to DNA is already known. We were able to discriminate between the two modes of pyrene binding; 7% of the pyrene binds to the minor groove whereas 93% intercalates. We used the new technique of Raman decoupling spectroscopy (see below) to selectively study this minor groove bound pyrene.

UV-Raman spectroscopy is, as yet, used in few analytical studies because the technique is practiced in only a few laboratories. Recently our laboratory examined unsaturation in polymer samples and demonstrated the sensitivity and selectivity obtainable with this technique. We were able to examine low concentrations of unsaturated species in polypropylene samples by exciting thin sheet samples at 220 nm where one would expect C=C enhancement to occur (*9*). The UV-Raman spectrum in Figure 6 is essentially identical to one that would be obtained by using excitation in the visible region, except for the new bands at 1590 (which turned out to be a contaminant) and 1640 cm^{-1}. The 1640 cm^{-1} band derives from C=C stretching.

Currently, it is difficult to relate concentrations to intensities because there are only a few UV-Raman cross sections measured. Quantitation requires the determination of the cross sections for each species of interest. In the case of unsaturation in olefins, we do not know the exact structure of the unsaturated species, and the cross section could be as small as 2 mBarns/molc sr (the C=C stretch of 1-hexene) or as large as 6 Barns/molc sr (the C=C stretch of 1,3-hexadiene) (*9*).

Given a cross section of ~ 100 μBarns/molc sr for the C–C stretching vibrations (*10, 11*), the concentration of the unsaturated species could be extremely low or as high as 1%. The UV absorption spectra indicate that the concentration is likely to be in the lower range. Thus, UV-Raman spectroscopy was useful for qualitative determinations of the presence of species that could not be determined by other in situ techniques. However, concentrations could not be determined from the intensities because the Raman cross sections were unknown for the analyte.

Other groups have also recently applied UV-Raman spectroscopy to analytical problems. K.P.J. Williams and D. Klenerman (*12*) studied petroleum samples and polymers, and P. B. Kelly et al. (*13*) demonstrated that particular carbon species can be observed in flames, a promising approach for studying combustion.

Biological studies

The number of applications of UV-Raman spectroscopy has grown fastest in biological areas such as the study of protein structure. In the past few years, the aromatic amino acid resonance Raman enhancement mechanisms have been elucidated and the dependence of the amino acid vibrational frequencies on environment (*14–21*) have been examined. The understanding of resonance enhancement of peptide backbone amide vibrations is evolving, and the major features of the dependence of the Raman spectra on peptide conformation are now known (*4, 22–29*).

Figure 7 illustrates the UV-Raman landscape of proteins, using myoglobin as an example. The figure shows the sperm whale myoglobin structure, the absorption spectrum of its fluoride complex, and its Raman spectra excited at different wavelengths within its visible and UV absorption spectrum.

Absorption in the near-UV and visible spectral regions derives solely from the heme group. Resonance Raman scattering, excited at 600 nm, occurs within a heme absorption band that contains charge transfer transitions involving the metal and

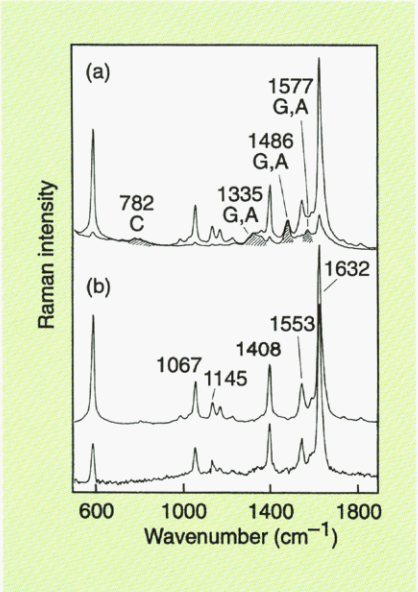

Figure 5. UV-Raman spectra of aqueous samples containing pyrene and calf thymus DNA excited at 244 nm with a continuous-wave laser.

(a) Upper spectrum obtained after SDS is added to sample. SDS extracts the pyrene into the micelles. Lower spectrum is sample prior to addition of SDS. The DNA bands are shaded and labeled according to their contribution from C, G, or A. (b) Same spectra as in (a) but with DNA contribution numerically removed. (Adapted from Reference 8.)

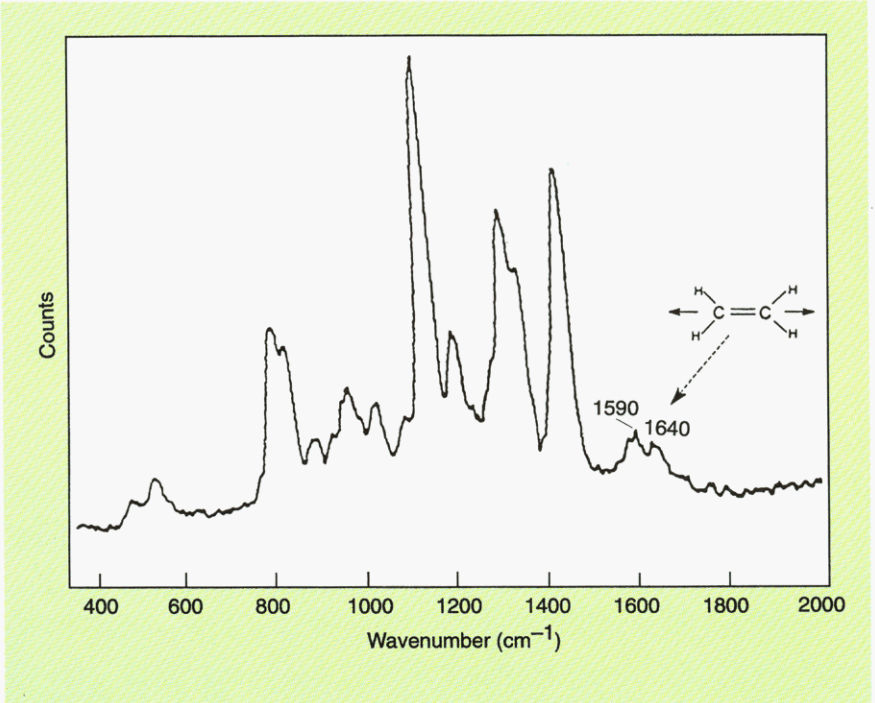

Figure 6. UV-Raman spectrum of a solid isotactic polypropylene sample excited at 220 nm.

The spectrum shows enhancement of a band at 1640 cm^{-1} from unsaturated species. (Adapted with permission from Reference 9.)

its ligands (*30*). These resonance Raman spectra in Figure 7 show strong bands from vibrations of heme in-plane ring breathing modes, as well as from iron–ligand diatomic-like iron–fluorine stretches. Excitation within the heme 400-nm $\pi \rightarrow \pi^*$ Soret band transition enhances only heme in-plane ring vibrations. No protein Raman bands are observed.

The absorption between 270 and 300 nm is contributed mainly by tryptophan (W) and tyrosine (Y) with a small contribution from phenylalanine (F). The large absorption increase between 260 and 220 nm mainly results from W and Y, and the increase below 220 nm derives mainly from the peptide backbone amide $\pi \rightarrow \pi^*$ transitions. Excitation of the Raman spectra of proteins in the 260–300 nm region results in the enhancement of aromatic amino acid Raman bands, but the spectral signal-to-noise ratio (S/N) is degraded because of fluorescence from W, Y, and F.

Much greater UV-Raman enhancement occurs for excitation within the strong W and Y absorption bands between 220 and 230 nm, and spectra are easily measured with very high S/N (Figure 7). Spectra excited below 220 nm result in enhancement mainly for the amide backbone vibrations. These amide Raman bands give information on the protein secondary structure because the frequencies and intensities are very sensitive to the protein folding. UV-Raman spectroscopy is arguably the most powerful technique for studying protein secondary structure at low protein concentrations.

UV-Raman spectroscopy has been used in many protein structural studies (*31–48*). An excellent example from Spiro's lab at Princeton (*31*) is a study of the hemoglobin cooperativity mechanism. Hemoglobin alters its quaternary structure in response to ligand binding to more efficiently transport oxygen. Spiro's work seeks to elucidate the coupling between ligand binding and protein structure.

Figure 8 shows the time dependence of the 230-nm UV resonance Raman spectra of the carbon monoxide complex of hemoglobin. Figure 8a shows the spectra of fully ligated carbon monoxyhemoglobin and deoxyhemoglobin, the form of the protein without ligands.

The lower spectrum in Figure 8a is the difference spectrum between

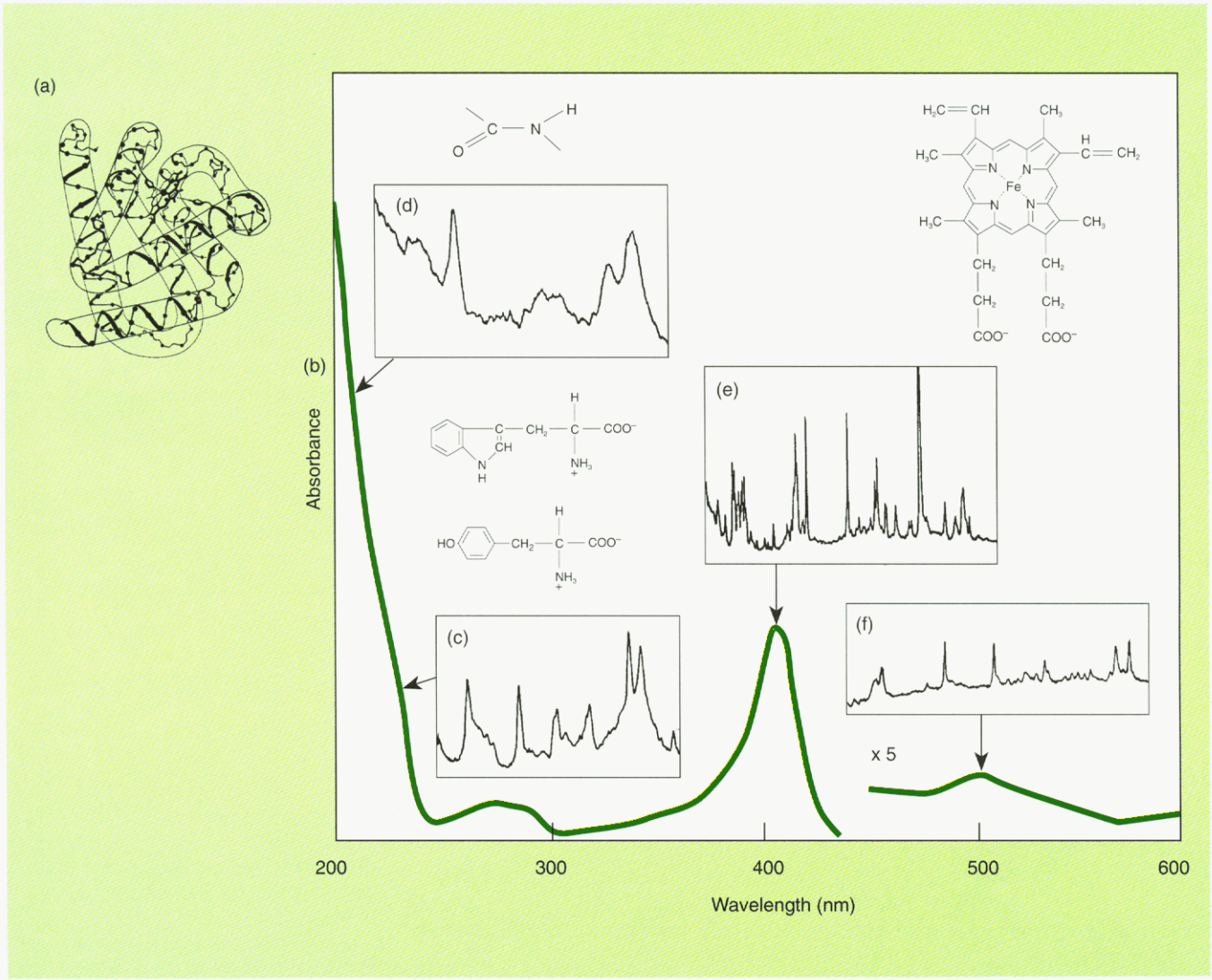

Figure 7. Resonance Raman protein landscape of sperm whale myoglobin.

(a) Myoglobin structure. (b) Absorption spectrum. (c) UV excitation at ~ 225 nm enhances tyrosine and tryptophan bands. (d) Excitation further in the UV region enhances amide vibrations whose intensities and frequencies depend on the protein secondary structure. Excitation within the heme absorption bands in the visible spectral region (400–600 nm) enhances vibrations only of (e) the heme ring and (f) those between the heme iron and its axial ligands. No protein vibrational modes are observed.

Figure 8. UV-Raman spectra of carbon monoxy- and deoxyhemoglobin excited at 230 nm.

(a) Upper spectra are carbon monoxyhemoglobin (HbCO) and deoxyhemoglobin (Hb); lower spectrum is the difference spectrum. (b) Difference spectra demonstrate evolution of the carbon monoxyhemoglobin spectra at various times subsequent to photolysis with a 419-nm pump pulse that flashes off the carbon monoxide ligand. Eventually the spectra evolve to the lower spectrum in (a). The bands are labeled with a letter and a number, indicating the type of amino acid and the vibrational mode assignment. (Adapted from Reference 31.)

deoxy- and oxyhemoglobin. Figure 8b shows a series of difference spectra, calculated by subtracting the spectra of static deoxyhemoglobin from that of samples of carbon monoxyhemoglobin photolyzed by 419-nm pulses of light.

Absorption of a 419-nm photon results in the rupture of the carbon monoxide–iron bond; the protein then begins a structural change toward the nonligated deoxyhemoglobin structure. The spectra show alterations of bands that derive from the hemoglobin W and Y residues. The spectra change with time in a complex manner. Hemoglobin contains numerous tryptophans and tyrosines; to elucidate protein structure alterations, it is crucial to relate the spectral changes to changes in

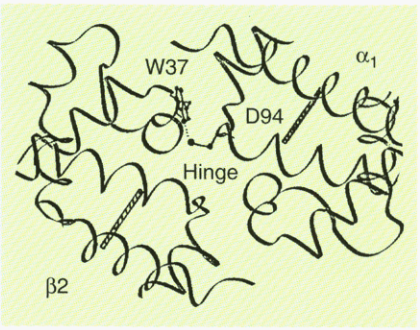

Figure 9. Cropped diagram of deoxyhemoglobin structure at the $\alpha_1\beta_2$ interface, showing the Trpβ37–Asp α94 (W37–D94) interaction.

Heme groups are indicated by the hashed bars and are seen end on. (Adapted from Reference 31.)

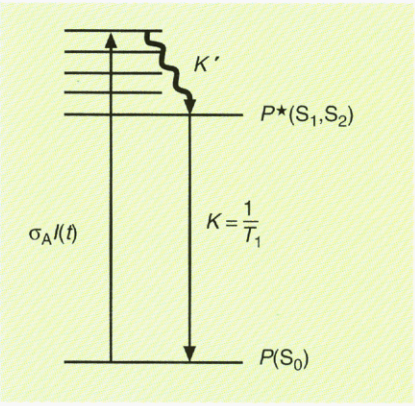

Figure 10. Energy-level diagram of kinetic model for Raman saturation phenomenon.

An incident photon flux of $I(t)$ is absorbed by the analyte molecules with an absorption cross section σ_A. The number of analyte molecules in the ground state is $P(S_o)$ and in the excited state is $P^*(S_1, S_2)$. K' is the electronic excited state vibrational relaxation rate to state P^*. The relaxation rate K to the ground state is the reciprocal of the T_1 recovery time.

the geometry and environment of particular W and Y amino acids in the protein. This is possible in some cases. For example, the W3 feature in Figure 9 has been assigned to a particular W known as the Trpβ37, an assignment made possible through mutant hemoglobin studies in which Trpβ37 was absent.

Figure 9 shows schematically the hemoglobin protein structure and the $\alpha_1\beta_2$ subunit interface that is considered important for transferring information between subunits on the ligation state of the hemes. Trpβ37 is thought be crucial to the cooperativity mechanism because it occurs at the $\alpha_1\beta_2$ interface hinge region. The Raman difference spectra indicate that alterations occur for most of the W and Y residue bands between the ligated and deoxyhemoglobin forms.

The kinetic difference Raman spectra in Figure 8 indicate that W other than the Trpβ37 are involved in the 30-ns prompt spectral changes. Alterations in Trpβ37 spectra are observed first in the 1-μs difference spectra. This result indicates that the tertiary subunit geometry changes initiated by the photolysis of the carbon monoxide ligand require an ~ 1-μs time interval to induce alterations at the distant Trpβ37 interface region. Careful studies of the Raman frequencies allow examination of hydrogen bonding changes for different W and Y residues. This study illustrates the power of UV resonance Raman spectroscopy to develop new molecular-bond-level information on complex biological systems.

The applications of UV-Raman spectroscopy to biological studies are rapidly expanding. Examples include studies of the existence of tyrosinates in bacteriorhodopsin (*35, 36, 40*), which may be involved in proton pumping. Other studies probe the conformation and structure of hormones and peptides in water and in lipid membranes (*49*). In addition, studies by Nelson's group (*50*) seek to examine algae and bacteria to identify the different species through their UV resonance Raman spectra.

New methods

Pulsed laser excitation causes nonlinear phenomena at high pulse energy fluxes. Ground-state depletion occurs even at the lowest pulse energy fluxes that give acceptable S/N Raman spectra if the analyte has nanosecond or longer excited-state lifetimes. The result is that the analyte band intensities are not linearly proportional to the incident pulse energy flux; as the pulse energy flux increases, the ground-state concentration decreases and the Raman intensities become saturated. If the populated excited state also has an absorption band at the excitation wavelength, new resonance Raman bands that derive from the excited-state species may be observed.

This saturation of the Raman intensities can be used to study excited-state relaxation processes. We developed a new technique called Raman saturation spectroscopy (*51, 52*), which can be used to monitor the saturation of the Raman intensities to determine the ground-state repopulation rate. This rate, which is equal to the reciprocal of the T_1 re-

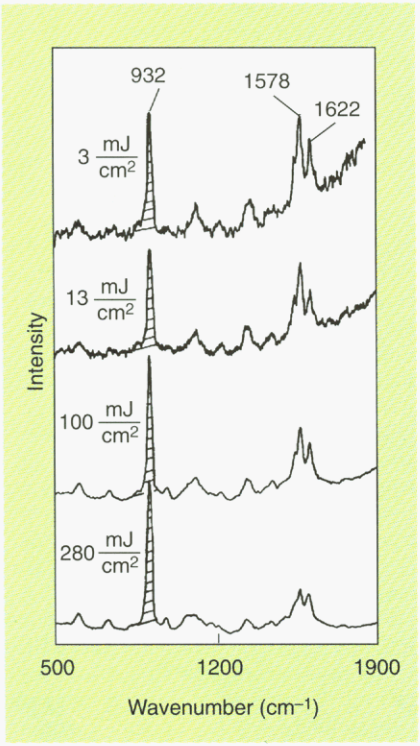

Figure 11. Raman saturation.

Raman intensities of tryptophanamide decrease as the incident laser pulse energy increases. The 932 cm^{-1} band is from the perchlorate internal standard. Excitation wavelength is 273 nm. Flux densities are indicated in the figure.

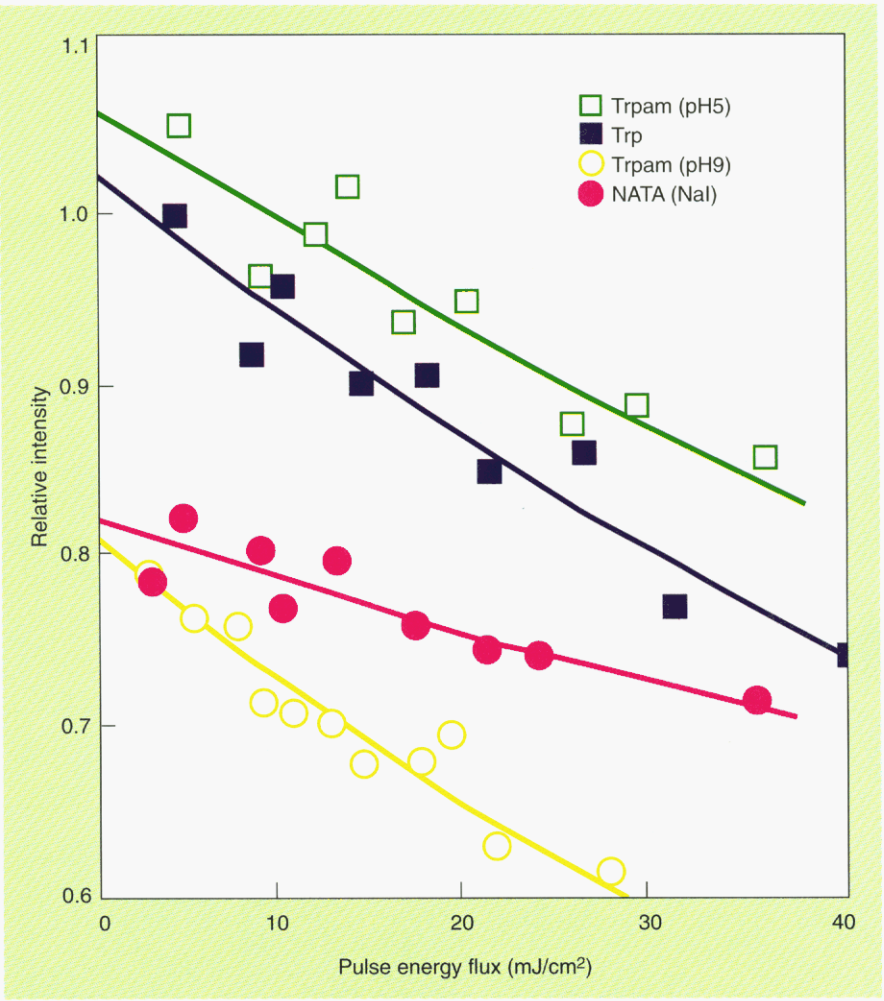

Figure 12. Raman saturation plots of tryptophan derivatives as a function of the pulse energy flux.

(Adapted from Reference 51.)

laxation time, will be equal to the reciprocal of the fluorescence lifetime if all ground-state repopulation occurs through the fluorescent excited state.

We developed a simple kinetic model from the energy-level diagram shown in Figure 10 that relates saturation of the Raman signal to the T_1 ground-state recovery time. The model has no adjustable parameters and requires only values for the incident pulse energy flux, the laser pulse width, the original analyte concentration, and the analyte absorption cross section.

The pulse energy flux dependence of the Raman band intensities relative to a nonabsorbing, nonphotochemically active internal intensity standard is measured. The T_1 relaxation time is determined by fitting the data to our model.

Raman saturation is evident from the dependence of the Raman spectra of tryptophanamide (Trpam) on the incident energy flux, as shown in Figure 11. The relative intensities of the tryptophanamide analyte bands at pH 9 excited in its S_1/S_2 transition at 273 nm relative to the 932-cm^{-1} perchlorate band decrease as the pulse energy flux increases.

Figure 12 shows Raman saturation plots of Trpam at pH 5 and pH 9, tryptophan at pH 7, and *N*-acetyltryptophanamide (NATA) in the presence of 0.5 M NaI, an excited-state fluorescence quencher. These data illustrate the pulse energy flux dependence of the relative intensities of the analyte bands on the intensity of the internal standard. The solid lines in the saturation plots are fits to the model; we determined T_1 lifetimes of 7 and 1.5 ns for Trpam, and 2 and 750 ps for tryptophan and NATA/NaI, respectively. The longer lived excited states show more saturation. The T_1 relaxation rate for these complexes is identical to the reciprocal of their measured fluorescence lifetimes.

We also measured the T_1 relaxation times excited at ~225 nm in the W S_3 excited state. In most cases we found the same T_1 repopulation rate. However, for Trpam at pH 5, we found an increased 3.5 ns T_1 lifetime, which is much longer than the fluorescence lifetime. This indicates the existence of a long-lived species that prevents Trpam from returning to the ground state. This intermediate appears to be a photoionized species that reversibly forms on photoexcitation of those W species with electrophilic substituents. The fluorescence data also indicate the existence of this intermediate through a decreased S_3 quantum yield.

Whereas the Raman saturation technique may, in some cases, give identical information to that obtained by fluorescence lifetime measurements, the Raman saturation technique has a major advantage in using a high-resolution probe that can resolve the lifetimes of species with overlapping fluorescence emission bands. In addition, because it monitors only the ground-state concentration, Raman saturation can measure excited state relaxation of nonfluorescent species. These species may form triplet-state intermediates, radical cations, or other photoionized species.

Fluorescence lifetime measurements in proteins are a standard approach for obtaining information on W and Y conformations, environments, and interresidue distances. In general, only W in proteins shows fluorescence because the Y residues transfer their excitation to the W through Förster energy transfer. The Raman saturation technique makes it possible, for the first time, also to study the excited-state lifetimes of Y and F. Furthermore, if the Raman bands can be resolved into contributions from individual aromatic amino acids, it would be possible to determine separately the excited-state lifetimes of each resolved residue.

Figure 13 shows the Raman saturation plots of the Y residues of glucagon, lysozyme, and myoglobin; we determined lifetimes of 50 ps, 6 ns, and 40 ps, respectively. In contrast, we determined the average W lifetimes to be 1.3 ns, 400 ps, and 70 ps, respectively (not shown). To our knowledge, these are the first Y lifetime measurements for these proteins. These are weighted average lifetimes of these amino acids in these proteins. Information on individual amino acid lifetimes can be obtained if we improve the S/N and deconvolute the contributions from different tryptophans and tyrosines.

This saturation method presents

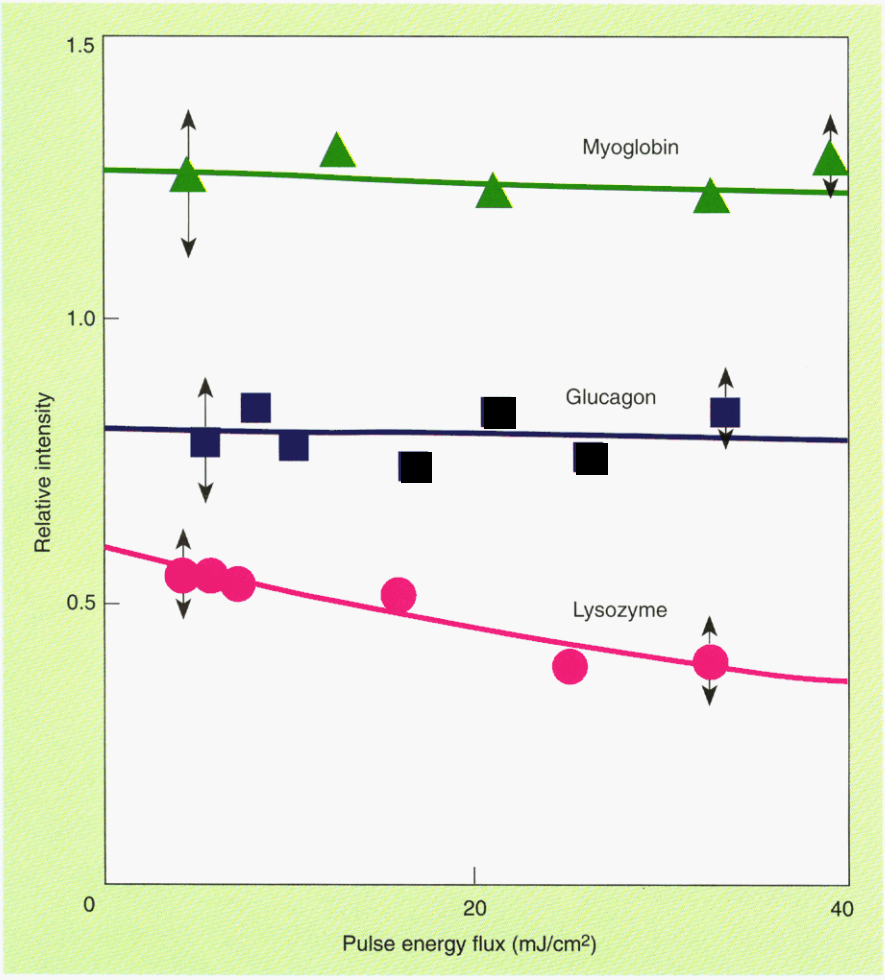

Figure 13. Raman saturation plots of the 1610 cm^{-1} band of tyrosine residues excited at 225 nm.

(Adapted from Reference 52.)

other opportunities. For example, saturation of the Raman spectra could be used to selectively remove contributions from particular species. We have demonstrated the usefulness of a technique we invented called Raman decoupling spectroscopy (*11*) and have used it to study separately the pyrene bound to the minor DNA groove in comparison with the pyrene that intercalates between bases. The intercalated pyrene has an extremely short T_1 lifetime and shows little saturation. In contrast, the minor groove bound pyrene has a relatively long lifetime.

A Raman difference spectrum between high and low pulse energy flux excitation displays the spectral features of the saturating minor groove bound pyrene, whereas the high-power spectrum is enriched in intercalated pyrene. The decoupling spectroscopy can use a multipulse sequence in which a pump pulse at a particular wavelength saturates one species, whereas a probe pulse interrogates the spectra of those molecules that remain in their ground state. We expect this technique to simplify the resonance Raman spectra of complicated samples.

Other techniques that will become increasingly important in the future include hyper-Raman scattering (*53*), where intense visible wavelength excitation at ν_0 results in scattering at a frequency of $2\nu_0-\nu_v$, spectra with high S/N, and new vibrations that can be especially sensitive to environment.

Future developments

Instrumental advances will make UV-Raman measurements easier. The intercavity doubled Ar^+ laser makes the UV-Raman measurement comparable in difficulty to the typical visible-wavelength Raman measurement. This continuous laser makes it possible to measure solid absorbing samples and to focus the beam to small diameters, allowing construction of a UV-Raman microscope.

Because the majority of molecules have UV absorption bands, it is now possible to apply resonance Raman spectroscopy to many problems. The combined application of UV, visible, and near-IR Raman excitation may become common. UV excitation selects for a small number of resonance-enhanced bands of an analyte and the measurements are made with high sensitivity and selectivity. In contrast, with nonresonance visible and near-IR excitation, numerous Raman bands occur with similar intensities for all components in the sample in proportion to their concentrations. Thus we will obtain both average and specific information on sample composition. The number of applications of UV-Raman spectroscopy is expanding rapidly as the technique finds new practitioners.

I gratefully acknowledge the contributions of the graduate students, postdocs, and colleagues who accomplished the work I have the pleasure of discussing here. In addition, I am especially indebted to Richard Bormett and John Holtz for helping me with this article and to Richard Bormett and Namjun Cho for allowing me to use their data before publication. I especially thank Foil Miller for helpful conversations and Tom Spiro and Bruce Hudson for allowing me to use their figures. We also gratefully acknowledge NIH grant 1R01GM30741 for funding this program.

References

(1) Asher, S. A. *Anal. Chem.* **1993**, *65*, 59–62.
(2) Asher, S. A.; Johnson, C. R. *Science* **1984**, *225*, 311–13.
(3) Asher, S. A. *Anal. Chem.* **1984**, *56*, 720–24.
(4) Johnson, C. R.; Asher, S. A. *Anal. Chem.* **1984**, *56*, 2258–61.
(5) Asher, S. A.; Jones, C. M. In *New Applications of Analytical Techniques to Fossil Fuels*; Perry, M.; Retcofsky, H., Eds.; ACS Symposium Series 31; American Chemical Society: Washington, DC, 1986; pp. 170–80.
(6) Jones, C. M.; Asher, S. A. *J. Chem. Phys.* **1988**, *89*, 2649–61.
(7) Rummelfanger, R.; Asher, S. A.; Perry, M. B. *Appl. Spectrosc.* **1988**, *42*, 267–72.
(8) Cho, N.; Asher, S. A., submitted for publication in *J. Am. Chem. Soc.*
(9) Killough, P. M.; DeVito, V. L.; Asher, S. A. *Appl. Spectrosc.* **1991**, *45*, 1067–69.
(10) Dudik, J. M.; Johnson, C. R.; Asher, S. A. *J. Chem. Phys.* **1985**, *82*, 1732–40.
(11) Dudik, J. M.; Johnson, C. R.; Asher, S. A. *J. Phys. Chem.* **1985**, *89*, 3805–14.
(12) Williams, K.P.J.; Klenerman, D. *J. Raman Spectrosc.* **1992**, *23*, 191.
(13) Getty, J. D.; Westre, S. G.; Bezebeh, D. Z.; Barrall, G. A.; Burmeister, M. J.; Kelly, P. B. *Appl. Spectrosc.* **1992**, *46*, 620.
(14) a. Asher, S. A.; Ludwig, M.; Johnson, C. R. *J. Am. Chem. Soc.* **1986**, *108*, 3186–97. b. Johnson, C. R.; Ludwig, M.; Asher, S. A. *J. Am. Chem. Soc.* **1986**, *108*, 905–12.
(15) Ludwig, M.; Asher, S.A. *J. Am. Chem. Soc.* **1988**, *110*, 1005–11.
(16) Sweeney, J.; Asher, S. A. *J. Phys. Chem.* **1990**, *94*, 4784–91.
(17) Johnson, C. R.; Ludwig, M.; O'Donnell, S.; Asher, S. A. *J. Am. Chem. Soc.* **1984**, *106*, 5008–10.
(18) Su, C.; Wang, Y.; Spiro, T. G. *J. Raman Spectrosc.* **1990**, *21*, 8179.
(19) Fodor, S.; Copeland, R.; Grygon, C.; Spiro, T. *J. Am. Chem. Soc.* **1989**, *111*, 5509.
(20) Rava, R.; Spiro, T. G. *J. Phys. Chem.* **1985**, *89*, 1856.
(21) Harada, I.; Takeuchi, H. In *Spectroscopy of Biological Systems*; Clark, R. T.; Hester, R. E., Eds.; John Wiley and Sons: New York, 1986.
(22) Hudson, B. S.; Mayne, L. C. In *Biological Applications of Raman Spectroscopy*; Spiro, T. G., Ed.; John Wiley and Sons: New York, 1987; Vol. II.

(23) Hudson, B.; Mayne, L. *Methods Enzymol.* **1986**, *130*, 331.
(24) Wang, Y.; Purrello, R.; Jordan, T.; Spiro, T. G. *J. Am. Chem. Soc.* **1989**, *111*, 8274–76.
(25) a. Wang, Y.; Purrello, R.; Jordan, T.; Spiro, T. G. *J. Am. Chem. Soc.* **1991**, *113*, 6359–68. b. Wang, Y.; Purrello, R.; Georgiou, S.; Spiro, T. *J. Am. Chem. Soc.* **1991**, *113*, 6368–77.
(26) Song, S.; Asher, S. A.; Krimm, S.; Bandekar, J. *J. Am. Chem. Soc.* **1988**, *110*, 8547–48.
(27) Krimm, S.; Song, S.; Asher, S. A. *J. Am. Chem. Soc.* **1989**, *111*, 4290–94.
(28) Song, S.; Asher, S. A. *J. Am. Chem. Soc.* **1989**, *111*, 4295–05.
(29) Song, S.; Asher, S. A.; Krimm, S.; Shaw, K. D. *J. Am. Chem. Soc.* **1991**, *113*, 1155–63.
(30) Asher, S. A. *Methods Enzymol.* **1981**, *76*, 372–413.
(31) Rodgers, K. R.; Su, C.; Subramanian, S.; Spiro, T. G. *J. Am. Chem. Soc.* **1992**, *114*, 3697–3709.
(32) Asher, S. A.; Larkin, P. J.; Teraoka, J. *Biochemistry* **1991**, *30*, 5944–54.
(33) Sweeney, J.; Harmon, P. A.; Asher, S. A.; Hutnik, C. M.; Szabo, A. G. *J. Am. Chem. Soc.* **1991**, *113*, 7531–37.
(34) Liu, G-Y.; Grygon, C. A.; Spiro, T. G. *Biochemistry* **1989**, *28*, 5046–50.
(35) Ames, J. B.; Bolton, S. R.; Netto, M. M.; Mathies, R. A. *J. Am. Chem. Soc.* **1990**, *112*, 9007–09.
(36) Harada, I.; Yamagishi, T.; Uchida, K.; Takeuchi, H. *J. Am. Chem. Soc.* **1990**, *112*, 2443–45.
(37) Hashimoto, S.; Ohsaka, S.; Takeuchi, H.; Harada, I. *J. Am. Chem. Soc.* **1989**, *111*, 8926–28.
(38) Efremov, R. G.; Feofanov, A. V.; Modyanov, N. N.; Nabiev, I. R. *FEBS Lett.* **1990**, *260*, 257.
(39) Toyama, A.; Kurashiki, E.; Watanabe, Y.; Takeuchi, H.; Harada, I. *J. Am. Chem. Soc.* **1991**, *113*, 3615.
(40) Netto, M.; Fodor, S.; Mathies, R. *Photochem. Photobiol.* **1990**, *52*, 605.
(41) Rava, R. P.; Spiro, T. G. *Biochemistry* **1985**, *24*, 1861.
(42) Copeland, R.; Spiro, T. *Biochemistry* **1985**, *24*, 4960.
(43) Hildebrandt, P.; Copeland, R.; Spiro, T.; Otlewski, J.; Laskowski, M.; Prendergast, F. *Biochemistry* **1988**, *27*, 5426.
(44) Copeland, R. A.; Spiro, T. G. *Biochemistry* **1987**, *26*, 2134–39.
(45) Copeland, R. A.; Spiro, T. G. *J. Am. Chem. Soc.* **1986**, *108*, 1281.
(46) Grygon, C. A.; Perno, J. R.; Fodor, S. P.; Spiro, T. G. *BioTech.* **1988**, *6*, 50.
(47) Kaminaka, S.; Kitagawa, T. *J. Am. Chem. Soc.* **1992**, *114*, 3256–60.
(48) Kaminaka, S.; Ogura, T.; Kitagawa, T. *J. Am. Chem. Soc.* **1990**, *112*, 23.
(49) Takeuchi, H.; Ohtsuka, Y.; Harada, I. *J. Am. Chem. Soc.* **1992**, *114*, 5321.
(50) Ghiamati, E.; Nelson, W.; Sperry, J. *Appl. Spectrosc.* **1992**, *46*, 357.
(51) Teraoka, J.; Harmon, P. A.; Asher, S. A. *J. Am. Chem. Soc.* **1990**, *112*, 2892–2900.
(52) Harmon, P. A.; Teraoka, J.; Asher, S. A. *J. Am. Chem. Soc.* **1990**, *112*, 8789–99.
(53) Ziegler, L. D.; Roebber, J. L. *Chem. Phys. Lett.* **1987**, *136*, 377–82.

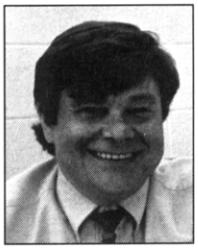

Sanford A. Asher is professor of chemistry and co-director of the Materials Research Center at the University of Pittsburgh, and adjunct professor of chemistry at Carnegie-Mellon University. He received his B.A. degree from the University of Missouri–St. Louis in 1971 and his Ph.D. from the University of California–Berkeley in 1977. He was a research fellow in applied physics at Harvard University between 1977 and 1980, and joined the University of Pittsburgh in 1980. Asher's research focuses on development of UV resonance Raman spectroscopy for fundamental and applied structural and trace studies of molecules in complex matrices and biological systems, and development of optical devices from self-assembling colloid particles.